NASA Technical Paper 3294

1993

Simulation of TunneLadder Traveling-Wave Tube Cold-Test Characteristics: Implementation of the Three-Dimensional, Electromagnetic Circuit Analysis Code Micro-SOS

Carol L. Kory
Ohio Aerospace Institute
Brook Park, Ohio

Jeffrey D. Wilson
Lewis Research Center
Cleveland, Ohio

NASA
National Aeronautics and Space Administration
Office of Management
Scientific and Technical Information Program

Summary

The three-dimensional, electromagnetic circuit analysis code, Micro-SOS, can be used to reduce expensive and time-consuming experimental "cold-testing" of traveling-wave tube (TWT) circuits. The frequency-phase dispersion characteristics and beam interaction impedance of a TunneLadder traveling-wave tube slow-wave structure were simulated using the code. When reasonable dimensional adjustments are made, computer results agree closely with experimental data. Modifications to the circuit geometry that would make the TunneLadder TWT easier to fabricate for higher frequency operation are explored.

Introduction

Micro-SOS is a three-dimensional, finite-difference, electromagnetic plasma physics simulation code that was developed by Mission Research Corporation (MRC) in cooperation with Varian Associates, Inc. (refs. 1 to 3). Micro-SOS is a version of the MRC code SOS (Self Optimized Sector) but differs in that it does not have the capability to simulate charged particle trajectories. It can be operated in either a time-domain algorithm in which Maxwell's time-dependent equations are solved, or a frequency-domain algorithm (as in this report) in which the resonant mode frequencies and field patterns are obtained.

Micro-SOS was developed by MRC as part of a DOD- and NASA-sponsored effort to develop software for microwave tube design. This code can provide a fast, inexpensive circuit analysis capability that can be used to obtain "cold-test" information about the electromagnetic fields in a microwave tube circuit. The term "cold-test" refers to evaluation of a circuit without the presence of an electron beam. Cold-test measurements are typically performed in the laboratory on actual- or scaled-size circuit models. Using Micro-SOS can potentially eliminate the need for these time-consuming and costly hardware cold-test measurements and greatly facilitate the design of novel microwave tube circuits.

In this report, Micro-SOS was used to determine the frequency-phase dispersion characteristics and beam interaction impedance of a TunneLadder traveling-wave tube (TWT) slow-wave circuit. We chose this circuit to simulate because it is capable of achieving high gain and power over a short distance and shows promise for a high-power, high-efficiency, relatively low-cost TWT at millimeter-wave frequencies. Because of its rather complex geometry, this circuit has not been previously analyzed with a high degree of accuracy.

Background

The TunneLadder is a millimeter-wave TWT with a fundamental forward-wave slow-wave circuit derived from the Karp circuit (refs. 4 and 5). The original Karp circuit (fig. 1) is a ridged waveguide with transverse slots in the top wall, with the slotted wall referred to as a "ladder." The radiofrequency (RF) field across the slots interacts with an electron beam that flows on either or both sides of the ladder. The passband of this circuit is above the cutoff frequency of the waveguide and below the frequency at which there is one-half wavelength between slots.

In the 1950's and early 1960's, the original Karp circuit was primarily used in backward wave oscillators (BWO's) at frequencies up to 300 GHz (refs. 5 to 7). When operated as a BWO, the beam voltage is adjusted to a level of only a few kilovolts so that the interaction takes place with the first backward space harmonic (fig. 2) at the intercept with the beam voltage line V_1. By increasing the beam voltage to V_2, the interaction takes place with the fundamental forward wave and the Karp circuit operates as an amplifier. Fundamental forward-wave interaction implies a higher rate of gain than that in backward-wave interaction. Karp (ref. 7) showed that this advantage can be enhanced in the TunneLadder circuit by forming the ladder into a quasi-elliptical shape, creating a beam tunnel through which the beam passes (fig. 3). The tunnel is supported by dielectric chips in a double-ridge waveguide. The resulting TunneLadder circuit is a narrow bandwidth, high-efficiency, mechanically sturdy, and relatively inexpensive millimeter-wave amplifier.

Kosmahl and Palmer (ref. 8) performed an approximate field analysis study of an idealized TunneLadder circuit. When a two-dimensional geometry was used, the beam tunnel was approximated by a circle and the dielectric supports were ignored. By approximately matching the axial electric and magnetic fields at circuit boundaries, frequency-phase dispersion curves were obtained that were in fairly good agreement with the experimental results obtained by Karp (ref. 7).

Two 29-GHz TunneLadder TWT's, fabricated and tested by Varian Associates, Inc., under contract to NASA Lewis Research Center (NAS3–22466) (ref. 9) successfully demon-

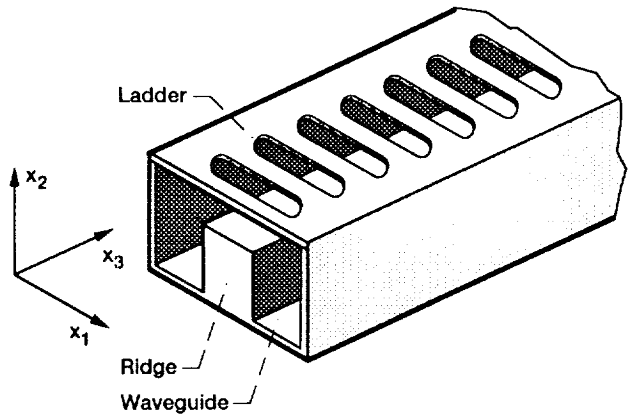

Figure 1.—Karp circuit.

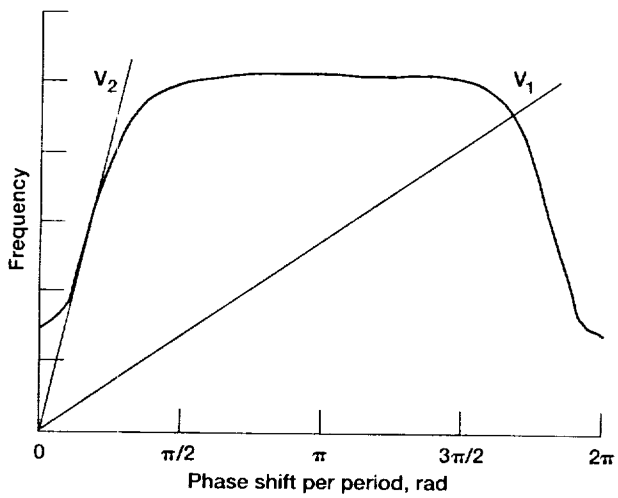

Figure 2.—Frequency-phase dispersion relationship for Karp circuit.

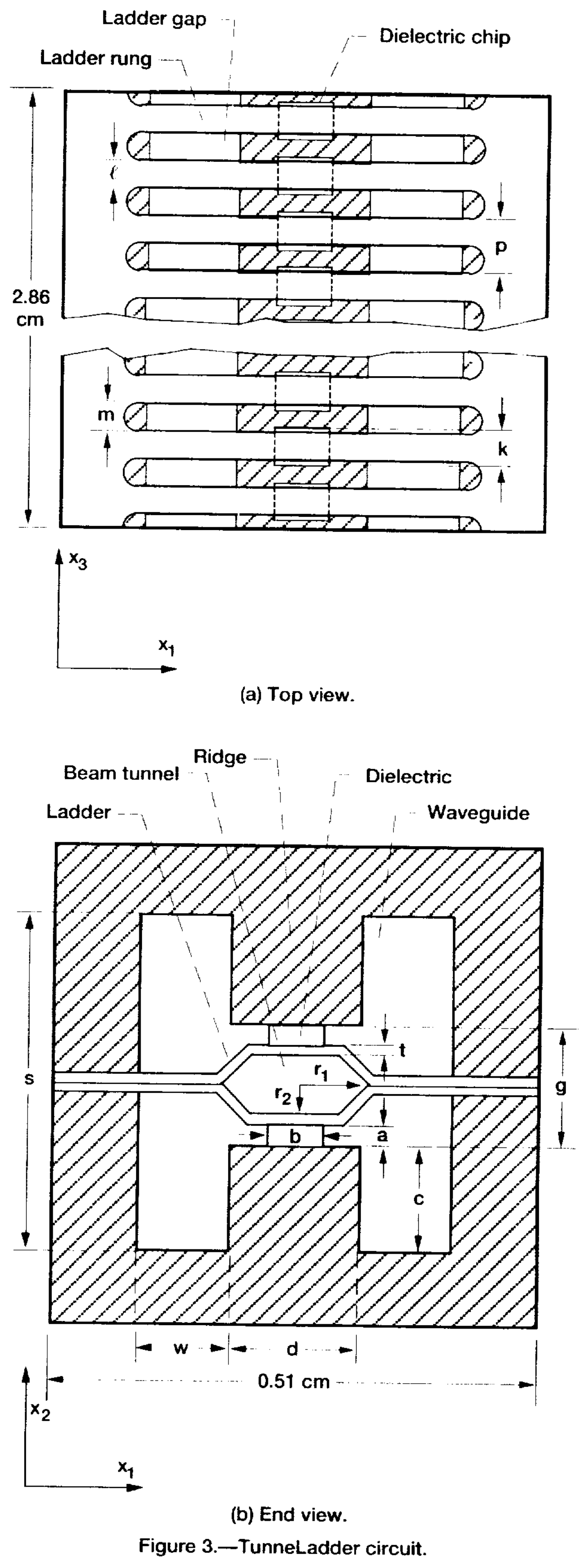

Figure 3.—TunneLadder circuit.

strated the high gain per length and interaction efficiency attainable with this narrow bandwidth circuit. The length of the slow-wave circuit was only 2.86 cm and the 10-kV, 215-mA electron beam was focused with a single permanent magnet. The first TWT (S/N 101) achieved a peak saturated RF output power of 365 W, a very high interaction efficiency of 17.0 percent, and a 3-dB bandwidth of 2.3 percent under pulsed operation. Because of an apparent vacuum leak, S/N 101 could not be operated under continuous wave (CW) conditions. The second TWT (S/N 102) was operational at CW, with a peak saturated RF output power of 316 W, interaction efficiency of 13.8 percent, and bandwidth of 2.8 percent. The lower values of efficiency and power for S/N 102 may have been due to a poor match in the output section. Despite these problems, the experimental results confirmed the high gain per length, high interaction efficiency, and narrow bandwidth characteristics predicted for the TunneLadder circuit.

In order to accurately simulate the electrical characteristics of the TunneLadder using a coupled-cavity, RF-electron beam interaction computer model (e.g., ref. 10), input is required for both beam interaction impedance and RF phase shift per cavity period. The frequency dependence of the RF phase shift per cavity period is known as the dispersion relationship. In the past, this information has been obtained experimentally by cold-test measurements of resonant frequencies of a short-circuited length of the circuit (refs. 11 to 13).

Karp (ref. 7) determined the dispersion characteristics for a TunneLadder circuit with an 8-period, cold-test model built to a 16:1 scale. Figure 4 shows the dispersion curves for the three lowest-order modes. The lowest frequency curve represents the symmetric ladder mode which provides for the useful gain of the circuit. In this mode, each ridge and ladder has the same RF potential as its opposite member across the beam hole, and the axial electric field is finite on the axis. The intersect of this curve with the diagonal line, representing the electron beam axial velocity, corresponds to the operating frequency and phase shift per period. The next highest frequency curve represents the undesirable antisymmetric ladder mode. In this mode, the RF potential at each ridge or ladder is 180° out-of-phase with its opposite member across the beam hole, and the axial electric field is zero on the axis. Interaction of the electron beam with this mode could produce undesired oscillation. However, because of the high frequency and weak axial electric field (except near the dielectric supports), circuit attenuation is higher than the gain, and the risk of oscillation is minimal (ref. 7). The circuit attenuation is even higher for the third mode (fig. 4), called the cavity mode, which is essentially the transverse magnetic mode TM_{11} that propagates in a double-ridge waveguide.

As shown herein, Micro-SOS can be used instead of experimental cold-testing to obtain dispersion characteristics and beam interaction impedance for the symmetric ladder mode of a TunneLadder circuit.

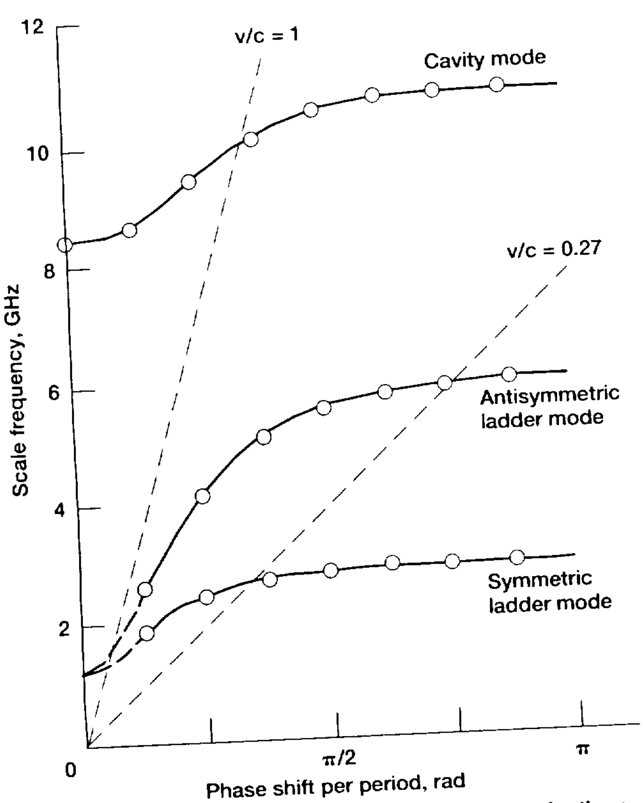

Figure 4.—Experimentally obtained dispersion curves for three lowest frequency modes of a TunneLadder circuit (from ref. 7).

Simulation

Micro-SOS was used to simulate the frequency-phase dispersion characteristics of the symmetric ladder mode of the Varian 29-GHz TunneLadder TWT (ref. 9) described in the previous section. The circuit is shown in figure 3 and the dimensions are given in table I. Figure 5 shows the $x_1 - x_2$ cross-sectional Micro-SOS grid with a single cavity divided into 37 (x_1-direction)×38 (x_2-direction)×8 (x_3-direction) cells, totaling 11 248 cells. The grid was nonuniform with the finest spacing in the beam hole region.

The procedure for calculating the dispersion characteristics is similar to that used by Kantrowitz and Tammaru (ref. 14) for a coupled-cavity circuit using the computer code ARGUS, a three-dimensional, electrodynamic circuit analysis code developed by Science Applications International Corporation (ref. 15). For a geometrically simpler coupled-cavity circuit, Kantrowitz and Tammaru obtained an accurate dispersion curve using only resonant frequencies at three different values of RF phase shift per cavity period. These resonances were obtained with three separate computer runs, each with different boundary conditions on a single cavity. To determine an accurate dispersion curve for the highly dispersive TunneLadder circuit, in addition to the three frequencies obtained with single-cavity Micro-SOS computations, two more resonant frequencies were obtained from a single computer run on a string of two cavities with the appropriate boundary conditions (described next).

TABLE I.—DIMENSIONS OF 29-GHZ TUNNELADDER CIRCUIT
[See fig. 3]

Parameter	Dimensions, mm
Dielectric height, a	0.2540
Dielectric width, b	.3810
Ridge height, c	1.0160
Ridge width, d	1.9050
Waveguide gap, g	1.2446
Dielectric length, k	.2032
Ladder length, l	.1524
Gap length, m	.1651
Period, p	.3175
Tunnel primary radius, r_1	.4300
Tunnel secondary radius, r_2	.3048
Side section height, s	3.2766
Ladder thickness, t	.0635
Side section width, w	.8890

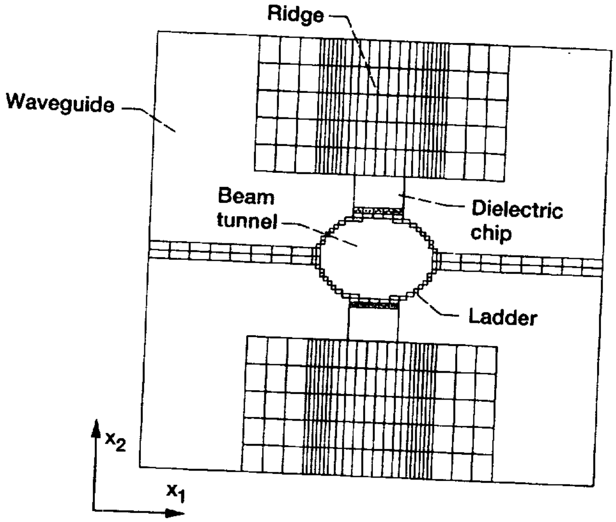

Figure 5.—Micro-SOS cross-sectional grid for TunneLadder circuit.

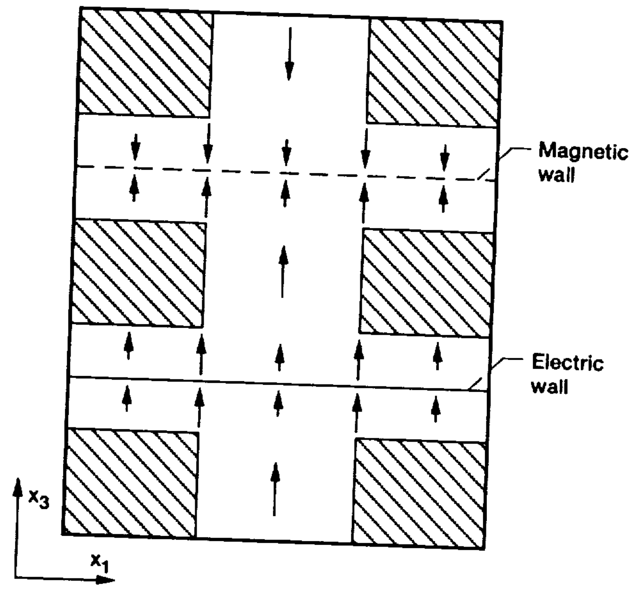

Figure 6.—Electric and magnetic wall boundary conditions for Micro-SOS.

In determining the resonance frequencies for both one- and two-cavity configurations, each axial boundary was truncated by either an "electric wall" or a "magnetic wall." An electric wall, E, is a boundary condition equivalent to a perfectly conducting plane at which the electric field is perpendicular and the magnetic field is parallel. With this boundary condition, the axial electric fields on each side of the boundary are in the same direction (fig. 6). It is simulated with Micro-SOS by using the STRUCTURE command. A magnetic wall, M, is a boundary condition that is a symmetry plane with parallel electric fields and perpendicular magnetic fields. With this boundary condition, the axial electric fields on the two sides of the boundary are in opposite directions (fig. 6). It is simulated with Micro-SOS by using the SYMMETRY command. Table II summarizes the boundary conditions used to obtain the various resonance points for the dispersion curve of the symmetric ladder mode. Table II also shows the run execution times consumed on Lewis' VAX minicomputer (model 9410). Additional resonance points could be obtained by modeling more than two cavities, but would require an excessive amount of computer time.

The beam interaction impedance, known as the Pierce interaction impedance, is a measure of the strength of interaction between an RF-wave space harmonic and the electron beam. For the fundamental space harmonic, the beam interaction impedance on the axis is given by (ref. 16)

$$K_{0,\text{axis}} = \frac{E_{z0}^2}{2\beta_0^2 P_{TOT}} \qquad (1)$$

where E_{z0} is the amplitude of the axial electric field of the fundamental space harmonic, β_0 is the axial phase constant for the fundamental space harmonic, and P_{TOT} is the total RF power flow given by

$$P_{TOT} = \frac{W_{TOT}}{NL} v_g \qquad (2)$$

where L is the cavity period, v_g is the group velocity, N is the number of cavities modeled, and W_{TOT} is the total electromagnetic energy stored in the cavities (obtained with Micro-SOS by using the BALANCE and OBSERVE commands). The group velocity for equation (2) is obtained by taking the derivative of the best-fitting polynomial curve to the dispersion data and is defined as

$$v_g = \frac{\partial\omega}{\partial\beta_0} = 2\pi L \frac{\partial f}{\partial(\beta_0 L)} \qquad (3)$$

where ω is angular frequency and f is frequency.

TABLE II. – MICRO-SOS RUNS WITH EXECUTION TIMES CONSUMED ON LEWIS' VAX MINICOMPUTER (MODEL 9410)

Cavities simulated	Boundary conditions	Phase, rad	Execution time, min:sec
1	E,E	π	4:25
1	E,M	$\frac{\pi}{2}$	15:08
1	M,M	0	16:41
2	E,M	$\frac{\pi}{4}, \frac{3\pi}{4}$	44:29

To obtain E_{z0} in equation (1), the LINPRINT command is used to print out the values of the axial electric field at the center of each grid cell along the z-axis at the center of the beam hole. The axial electric field is then Fourier analyzed to determine E_{z0}.

Note that the beam interaction impedance given in equation (1) is the value on the axis. In simulations with an RF-beam interaction coupled-cavity TWT model, such as in reference 10, one must input the impedance integrated over the beam cross-section area. With the radial variation of the fundamental space harmonic of the electric field given by $I_0(\gamma_0 r)$ (ref.17, p. 28), the finite beam interaction impedance is given by

$$K_{0,\text{beam}} = K_{0,\text{axis}}\left[I_0^2(\gamma_0 b) - I_1^2(\gamma_0 b)\right] \tag{4}$$

where $K_{0,\text{axis}}$ is given by equation (1), b is the beam radius, I_0 and I_1 are the modified Bessel functions, and γ_0 is the radial propagation constant for the fundamental space harmonic

$$\gamma_0 = \sqrt{\beta_0^2 - \frac{\omega^2}{c^2}} \tag{5}$$

Results

Baseline TunneLadder Circuit

When first modeled with the exact dimensions from reference 9, the symmetric ladder mode resonance at phase $\beta L = \pi$ occurred at 29.5 GHz, which is 6.35 percent under the experimental value of 31.5 GHz. By decreasing the thickness of the ladder between the beam hole and dielectric support by only 0.031 mm, with a simultaneous increase in the height of the dielectric chip from 0.254 to 0.285 mm (the shaded grid cells in figure 5 were replaced with dielectric), the calculated resonance frequency matched the experimental value. This change in ladder thickness can be justified because of the nature of the TunneLadder construction. When the Type IIA diamond chips are brazed onto the soft Amzirc ladder, they are very likely partially driven into the metal, decreasing the ladder thickness. To obtain a dispersion curve, resonant frequencies were obtained at phases of 0, $\pi/4$, $\pi/2$, and $3\pi/4$ in addition to that at π by using the cavity configurations and boundary conditions given in table II. The Micro-SOS input file used to obtain the resonant frequency at a phase of $\pi/2$ is given in appendix A, and the input file used to obtain the resonant frequencies at phases $\pi/4$ and $3\pi/4$ is given in appendix B.

In addition to calculating the resonant frequencies, Micro-SOS can plot the electric field at any specified location using the VECTOR command. For example, the electric field pattern for the symmetric ladder mode at the $\pi/4$ resonance point is shown in figure 7(a) for an $x_1 - x_3$ cross-section on the axis, and in figure 7(b) for an $x_1 - x_2$ cross-section through the center of a gap.

The dispersion curve for the symmetric ladder mode is obtained by plotting the calculated resonance points of table III (case 1) in figure 8. As shown, the agreement with the experimental results obtained from cold-test measurements (ref. 9) is very high, demonstrating the accuracy of the Micro-SOS simulation.

After the dispersion curve has been obtained, the beam interaction impedance can be calculated from equation (1). Table IV gives the parameters obtained from Micro-SOS that were used to calculate the impedance for three different values of phase. Figure 9 (case 1) shows that the impedance decreases with an increasing phase shift per cavity. There were no experimental data to compare the impedance values with, but the formulation for calculating the impedance has been verified with calculated results compared with data from a ferruleless coupled-cavity TWT circuit (ref. 18).

Dielectric Rod Circuit

If the TunneLadder circuit is to be used at higher frequencies, the decrease in size would make accurate positioning of the dielectric chips extremely difficult. Fabrication would be much easier if the chips were replaced by two continuous dielectric rods. However, such an increase in the dielectric loading of a slow-wave circuit increases the capacitance, with expected deleterious consequences of decreased phase velocity (decreased frequency at a given phase) and impedance (ref. 12, pp. 43 to 45).

The Micro-SOS calculations shown in table III and figure 8 (case 2) confirm that the increased dielectric loading decreases the phase velocity, with the frequency decrease ranging from 1.02 GHz (6.33 percent) at a phase of zero to 3.07 GHz (9.75 percent) at a phase of π rad. However, contrary to our expectations, the impedance calculated in table IV and shown in figure 9 (case 2) actually increased, rising 16.9 percent from 121.4 to 141.9 Ω at a phase of $\pi/2$ rad. The impedance increase can be explained by the added dielectric decreasing the frequency more at larger values of phase than at smaller values. This causes a flattening of the

TABLE III.—FREQUENCY-PHASE DISPERSION CALCULATIONS

Case	Dielectric	Side width, mm	Phase, rad				
			0	$\frac{\pi}{4}$	$\frac{\pi}{2}$	$\frac{3\pi}{4}$	π
			Frequency, GHz				
1	Chips	0.8890	16.12	26.91	30.33	31.27	31.50
2	Rods	.8890	15.10	24.73	27.54	28.26	28.43
3	Rods	.6595	17.08	27.28	30.46	31.30	31.51

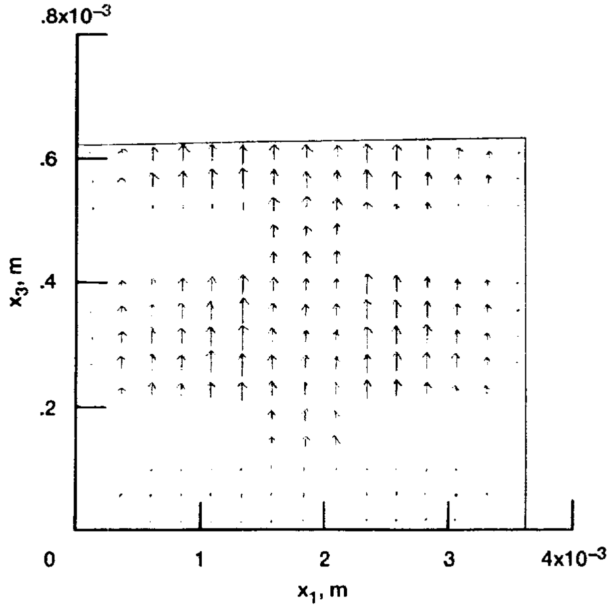

(a) Top view.

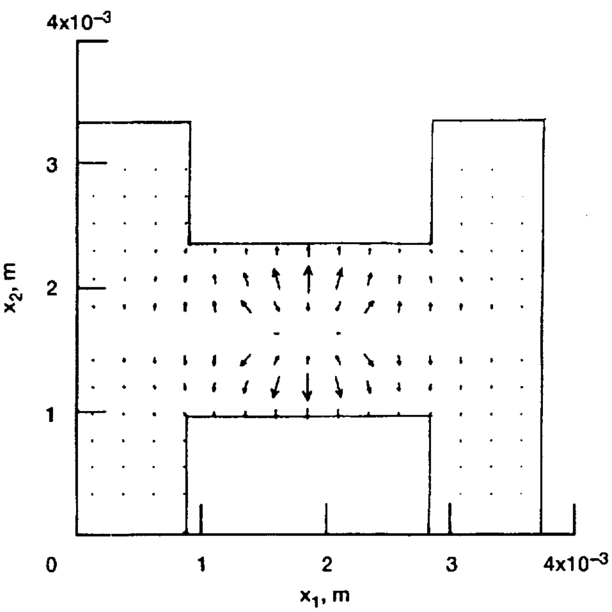

(b) End view.

Figure 7.—Calculated electric field in symmetric ladder mode of TunneLadder circuit at a phase of $\pi/4$.

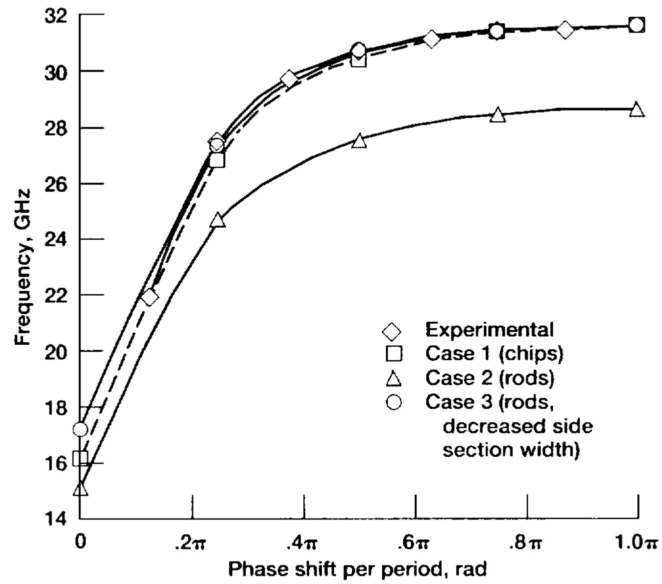

Figure 8.—Dispersion relationship for symmetric ladder mode of TunneLadder circuit.

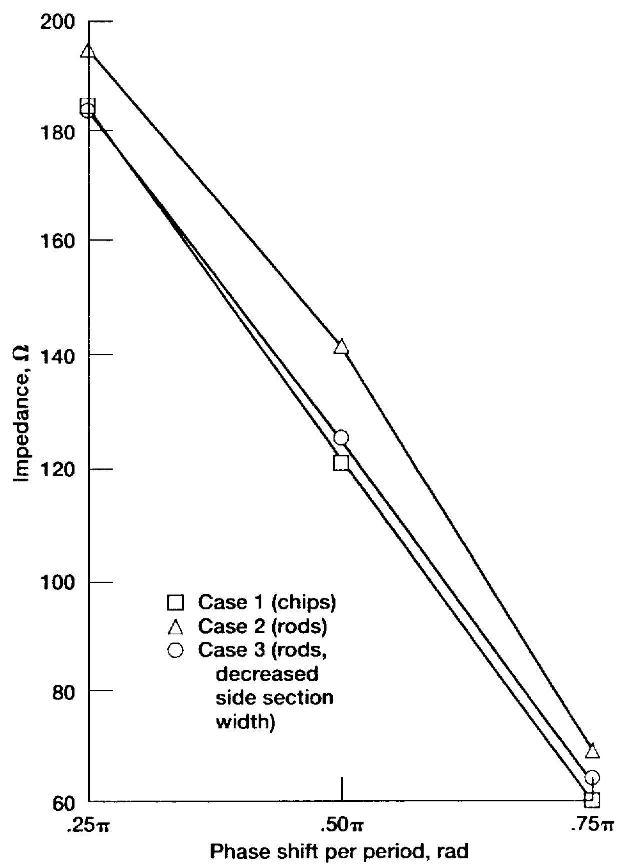

Figure 9.—Calculated beam interaction impedances for TunneLadder circuits.

dispersion curve (fig. 8) with resulting decreases in the group velocity and bandwidth. The group velocity, which is inversely proportional to the impedance, decreased 23.7 percent, whereas $E_{z0}^2 \, NL/W_{TOT}$, which is proportional to the impedance, decreased only 10.8 percent. Thus, there was a net increase in impedance.

To more accurately assess the effects of replacing the dielectric support chips with rods, circuits were compared at approximately equal operating frequencies by altering the waveguide geometry of the TunneLadder circuit. As a guideline to altering the dimensions, an approximate relationship for the cutoff frequency of a double-ridge waveguide (ref. 19, p. 470),

TABLE IV. – BEAM INTERACTION IMPEDANCE

Case	Parameter	Phase, rad		
		$\frac{\pi}{4}$	$\frac{\pi}{2}$	$\frac{3\pi}{4}$
1	Frequency, GHz	27.10	30.59	31.38
	E_{z0}^2NL/W_{TOT} (10^6 V^2/Jm)	3.522	2.418	.8477
	Group velocity (10^6 m/s)	15.56	4.066	1.282
	Impedance, Ω	184.8	121.4	60.0
2	Frequency, GHz	24.82	27.69	28.32
	E_{z0}^2NL/W_{TOT} (10^6 V^2/Jm)	3.193	2.156	.760
	Group velocity (10^6 m/s)	13.36	3.101	.992
	Impedance, Ω	195.2	141.9	69.6
3	Frequency, GHz	27.41	30.64	31.40
	E_{z0}^2NL/W_{TOT} (10^6 V^2/Jm)	3.294	2.259	.794
	Group velocity (10^6 m/s)	14.59	3.699	1.137
	Impedance, Ω	184.4	124.7	63.4

$$f_c = \frac{1}{2\pi}\left(\frac{2g}{\mu\varepsilon wsd}\right)^{\frac{1}{2}} \qquad (6)$$

was used, where μ is the permeability, ε is the permittivity, and g, w, s, and d are waveguide dimensions shown in figure 3. To increase the frequency, we chose to alter the side section width w. As shown in figure 8 and table III, a dielectric rod circuit with w decreased by 25.8 percent (case 3) had a dispersion curve very similar to that of the original dielectric chip circuit (case 1). The calculated beam interaction impedance is also very similar as shown in figure 9 and table IV. Thus, a dielectric rod circuit with decreased side section width was shown to be very similar to a dielectric chip circuit with respect to dispersion and impedance.

Conclusions

The usefulness of the electromagnetic circuit analysis computer code Micro-SOS in reducing the need for expensive and time-consuming experimental cold-testing in the design process for traveling-wave tube circuits was demonstrated. The code was used to calculate the frequency-phase dispersion characteristics and beam interaction impedance of a TunneLadder traveling-wave tube slow-wave structure. After making minor, justifiable adjustments in the dimensions of the ladder, computational results agreed very closely with experimental data.

While the TunneLadder TWT simulated in this study operated at a frequency of 29 GHz, this type of circuit is being considered for future use at higher frequencies. Because of the smaller circuit dimensions at higher frequencies, positioning of the dielectric chip ladder supports as used in the 29-GHz circuit would be extremely difficult. Thus, simulations were made with the chips replaced by a pair of rods that are much easier to position accurately. Because of the increased dielectric loading of the rods, frequency, the ordinate of the dispersion curve, was decreased. However, one can compensate for this decrease in frequency by decreasing the side section widths. Thus, a modified TunneLadder circuit with decreased side section widths and a ladder supported by continuous dielectric rods could have approximately the same gain and efficiency but with a smaller bandwidth than the original circuit supported with dielectric chips.

Lewis Research Center
National Aeronautics and Space Administration
Cleveland, Ohio, September 28, 1992

References

1. Goplen, B.; McDonald, J.; and Warren, G.: SOS Reference Manual Version October 1988. Mission Research Corporation, Mar. 1989.
2. Goplen, B., et al.: SOS User's Manual Version October 1988. Mission Research Corporation, Mar. 1989.
3. Doniger, K.J., et al.: Standard Problem Set for Micro-SOS Electromagnetic Circuit Modeling Code Version October 1988. Varian Associates, Inc., Mar. 1989.
4. Karp, A.: Traveling-Wave Tube Experiments at Millimeter Wavelengths with a New, Easily Built, Space Harmonic Circuit. Proc. IRE, vol. 43, Jan. 1955, pp. 41–46.
5. Karp, A.: Backward-Wave Oscillator Experiments at 100 to 200 Kilomegacycles. Proc. IRE, vol. 45, Apr. 1957, pp. 496–503.
6. Cohen, L.D.: Backward-Wave Oscillators for the 50- to 300-GHz Frequency Range. IEEE Trans. Electron Devices, vol. ED-15, no. 6, June 1968, pp. 403–404.
7. Karp, A.: Design Concepts for a High-Impedance Narrow-Band 42 GHz Power TWT Using a Fundamental /Forward Ladder-Based Circuit. NASA CR-165282, 1980.
8. Kosmahl, H.G.; and Palmer, R.W.: Harmonic Analysis Approach to the "TunneLadder": A Modified Karp Circuit for Millimeter-Wave TWTA's. IEEE Trans. Electron Devices, vol. ED-29, no. 5, May 1982, pp. 862–869.
9. Jacquez, A., et al.: A Millimeter-Wave TunneLadder TWT. NASA CR-182184, 1988.
10. Wilson, J.D.: Revised NASA Axially Symmetric Ring Model for Coupled-Cavity Traveling-Wave Tubes. NASA TP-2675, 1987.
11. Nalos, E.J.: Measurement of Circuit Impedance of Periodically Loaded Structures by Frequency Perturbation. Proc. IRE, vol. 42, 1954, pp. 1508–1511.
12. Gittins, J.F.: Power Travelling-Wave Tubes. American Elsevier Publishing Co., New York, 1965.
13. Horsely, A.W.; and Pearson, A.: Measurement of Dispersion and Interaction Impedance Characteristics of Slow-Wave Structures by Resonance Methods. IEEE Trans. Electron Devices, vol. ED-13, no. 12, Dec. 1966, pp. 962–969.
14. Kantrowitz, F.; and Tammaru, I.: Three-Dimensional Simulations of Frequency-Phase Measurements of Arbitrary Coupled-Cavity RF Circuits. IEEE Trans. Electron Devices, vol. ED-35, no. 11, Nov. 1988, pp. 2018-2026.

15. Mondelli, A., et al.: ARGUS Code Manual User's Guide. Science Applications International Corporation, Apr. 1, 1991.
16. Gewartowski, J.W.; and Watson, H.A.: Principles of Electron Tubes. D. Van Nostrand Company, Inc., 1965, p. 357.
17. Pierce, J.R.: Traveling-Wave Tubes. D. Van Nostrand Company, Inc., 1950.
18. Schroeder, D.L.; and Wilson, J.D.: Ferruleless Coupled-Cavity Traveling-Wave Tube Cold-Test Characteristics Simulated with Micro-SOS. NASA TP-3306, 1993.
19. Ramo, S.; Whinnery, J.R.; and Van Duzer, T.: Fields and Waves in Communication Electronics, Second ed., John Wiley and Sons, 1984.

Appendix A
Input File for $\pi/2$ Phase

```
TITLE * TUNNELADER CIRCUIT, 1 CAV, 1 SYMMETRY * /

COMMENT * THE GRID SPACING IS IDENTIFIED THROUGH THE X1GRID, X2GRID, AND
          X3GRID COMMANDS.  SINCE THE SPACING IS NOT UNIFORM, FUNCTION IS
          USED IN THE COMMAND.  THE CELLS ARE LARGE IN THE AREAS OF LITTLE
          SIGNIFICANCE AND VERY FINE IN THE AREAS WHERE THE ELECTRIC FIELDS
          ARE STRONG. * /
X1GRID FUNCTION 38 1 .00  5 .0001778 .000889
                          3 .000153 .000459
                          2 .00003175 .0000635
                          4 .0000325 .00013
                          2 .00005475 .0001095
                          5 .0000762 .000381
                          2 .00005475 .0001095
                          4 .0000325 .00013
                          2 .00003175 .0000635
                          3 .000153 .000459
                          5 .0001778 .000889 /

X2GRID FUNCTION 40 1 0.00 5 .0002032 .001016
                          2 .0001143 .0002286
                          1 .0000254 .0000254
                          2 .00003175 .0000635
                          8 .0000301625 .0002413
                          3 .00004233 .000127
                          8 .0000301625 .0002413
                          2 .00003175 .0000635
                          1 .0000254 .0000254
                          2 .0001143 .0002286
                          5 .0002032 .001016 /

COMMENT * THE FULL LENGTH OF X3 IS .0003175 m * /
X3GRID FUNCTION 9 1 0.00  1 .0000762 .0000762
                          1 .0000254 .0000254
                          4 .00002857 .0001143
                          1 .0000254 .0000254
                          1 .0000762 .0000762 /


COMMENT * THE SYMMETRY COMMAND CREATES A "MAGNETIC" WALL AT THE BOUNDARY.
          BY EDITING THIS SECTION, THE PI, PI/2, AND 0 PHASE SHIFTS ARE
          OBTAINED. * /
SYMMETRY MIRROR          +1 1 38 1 40 1 1 /
C SYMMETRY MIRROR          -1 1 38 1 40 9 9 /
```

```
COMMENT * THE ENTIRE GRID SPACE IS BLOCKED AS WELL AS ONE CELL LAYER
          ON EACH SURROUNDING WALL.  THIS CREATES A PERFECT CONDUCTOR
          AT EACH BOUNDARY. * /
STRUCTURE CONFORMAL BLOCK +1 0 39 0 41 0 10 /


COMMENT * HOLLOW OUT THE DOUBLE RIDGE * /
STRUCTURE CONFORMAL LEFTLEG -1 1 6 1 40 1 9 /
STRUCTURE CONFORMAL RIGHTLEG -1 33 38 1 40 1 9 /
STRUCTURE CONFORMAL CENTER -1 6 33 6 35 1 9 /


COMMENT * ADD THE DIELECTRIC IN THE CENTER OF THE STRUCTURE BENEATH THE
          BEAMHOLE * /
DIELECTRIC NO NULL 5.5 0.0 0.0 17 22 6 10 1 3 /
DIELECTRIC NO NULL 5.5 0.0 0.0 17 22 31 35 1 3  /
DIELECTRIC NO NULL 5.5 0.0 0.0 17 22 6 10 7 9 /
DIELECTRIC NO NULL 5.5 0.0 0.0 17 22 31 35 7 9 /


COMMENT *FORM THE BEAMHOLE APPROXIMATING IT AS AN ELLIPSE.  THE ENTIRE
         BEAM IS FORMED AS A SOLID FIRST AND THEN HOLLOWED TO ACHIEVE THE
         PROPER THICKNESS OF THE BEAM TUNNEL.* /
STRUCTURE ELLIPTICAL BEAMFILL +1 CARTESIAN .0018453 .0016383 0.0
                                 .0018453 .0016383 .0003174
                                 1 0 0 .00046175 .00033655
                                 1 0 0 .00046175 .00033655
                                 0 360 0 360 /

STRUCTURE ELLIPTICAL BEAMHOLE -1 CARTESIAN .0018453 .0016383 0.0
                                 .0018453 .0016383 .0003174
                                 1 0 0 .00043 .0003048
                                 1 0 0 .00043 .0003048
                                 0 360 0 360/

STRUCTURE ELLIPTICAL SLOT1 -1 CARTESIAN .0018453 .0016383 .0000762
                                 .0018453 .0016383 .0002413
                                  1 0 0 .00046175 .00033655
                                  1 0 0 .00046175 .00033655
                                  0 360 0 360 /


COMMENT * FORM THE LADDER * /
STRUCTURE CONFORMAL LADDERLEFT +1 0 10 19 22 1 9 /
STRUCTURE CONFORMAL LADDERRIGHT +1 29 39 19 22 1 9 /
STRUCTURE CONFORMAL SLOT2 -1 1 10 19 22 2 8 /
STRUCTURE CONFORMAL SLOT3 -1 29 38 19 22 2 8 /
```

```
COMMENT * ONE RESONANT FREQUENCY IS REQUESTED. THE MAXIMUM FREQUENCY,
          IN THIS COMMAND SET TO 35 GHZ, SHOULD BE APPROXIMATELY
          10% ABOVE THE EXPECTED MAXIMUM FREQUENCY. * /
FREQUENCY 1 35E+9 .005 50000 /
DIAGNOSE FREQUENCY 1 0 1 /


COMMENT * THE BALANCE AND OBSERVE COMMANDS ARE USED TOGETHER TO CALCULATE THE
          TOTAL ENERGY IN THE MODELED STRUCTURE.  THIS VALUE OF ENERGY IS USED
          IN THE IMPEDANCE CALCULATIONS.  *
BALANCE 1 1 38 1 40 1 9 /
OBSERVE 1 YES ENERGY 1 0.0 0.0 0.0 0.0 TOTAL 0 1 /


COMMENT * THE LINPRINT COMMAND PRINTS OUT THE VALUES OF THE FIELD IN THE
          SPECIFIED REGION.  THIS COMMAND WILL PRINT OUT THE AXIAL ELECTRIC
          FIELD AT THE CENTER OF THE BEAMHOLE. * /
LINPRINT 1 3 2 1 19 19 20 20 1 9 0 0 1 0 0 0 0 0 0 /


COMMENT * THE RANGE COMMAND PLOTS THE FIELD VALUES THAT THE LINPRINT
          COMMAND PRINTS OUT.  THE AXIAL ELECTRIC FIELD IS PLOTTED IN
          THIS COMMAND.  THIS PLOT IS FOURIER ANALYZED TO OBTAIN THE
          EFFECTIVE FIELD SEEN BY THE BEAM AND USED TO CALCULATE THE
          PIERCE INTERACTION IMPEDANCE. * /
RANGE 1 1 0 0 3 19 19 20 20 1 9 /


COMMENT * THE VECTOR COMMAND PLOTS THE RF FIELDS IN THE 2-DIMENSIONAL
          AREA SPECIFIED. * /
COMMENT * ELECTRIC FIELD IN THE X-Y PLANE THROUGH THE LADDER * /
VECTOR  1 1 1 1 E X1 X2 0.0 .003683 0.0 .003277 .0002413 .0002413 15 15 /

COMMENT * X-Y PLANE THROUGH THE SLOT * /
VECTOR 1 1 1 1 E X1 X2 0.0 .003683 0.0 .003277 .0001587 .0001587 15 15 /

COMMENT * Y-Z PLANE THROUGH THE RIDGE * /
VECTOR 1 1 1 1 E X2 X3 .0005334 .0005334 0.0 .003277 0.0 .0003175 15 15 /

COMMENT * TOP VIEW THROUGH THE CENTER * /
VECTOR 1 1 1 1 E X3 X1  0.0 .003683 .001638 .001638 0.0 .0003175 15 15 /

COMMENT * TOP VIEW THROUGH A DIELECTRIC * /
VECTOR 1 1 1 1 E X3 X1 0.0 .003683 .0021461 .001461 0.0 .0003175 15 15 /


START /
STOP /
```

Appendix B
Input File for $\pi/4$ and $3\pi/4$ Phases

```
TITLE *TUNNELADDER CIRCUIT, 2 CAV, 1 SYMMETRY * /

X1GRID FUNCTION 38 1 .00  5 .0001778 .000889
                          3 .000153 .000459
                          2 .00003175 .0000635
                          4 .0000325 .00013
                          2 .00005475 .0001095
                          5 .0000762 .000381
                          2 .00005475 .0001095
                          4 .0000325 .00013
                          2 .00003175 .0000635
                          3 .000153 .000459
                          5 .0001778 .000889 /

X2GRID FUNCTION 40 1 0.00 5 .0002032 .001016
                          2 .0001143 .0002286
                          1 .0000254 .0000254
                          2 .00003175 .0000635
                          8 .0000301625 .0002413
                          3 .00004233 .000127
                          8 .0000301625 .0002413
                          2 .00003175 .0000635
                          1 .0000254 .0000254
                          2 .0001143 .0002286
                          5 .0002032 .001016 /

COMMENT * THE FULL LENGTH OF X3 IS .000635 m * /
X3GRID FUNCTION 17 1 0.00 1 .0000762 .0000762
                          1 .0000254 .0000254
                          4 .000028575 .0001143
                          1 .0000254 .0000254
                          2 .0000762 .0001524
                          1 .0000254 .0000254
                          4 .000028575 .0001143
                          1 .0000254 .0000254
                          1 .0000762 .0000762    /

STRUCTURE CONFORMAL BLOCK +1 0 39 0 41 0 18 /
STRUCTURE CONFORMAL LEFTLEG -1 1 6 1 40 1 17 /
STRUCTURE CONFORMAL RIGHTLEG -1 33 38 1 40 1 17 /
STRUCTURE CONFORMAL CENTER -1 6 33 6 35 1 17 /

CQMMENT * ADD THE DIELECTRIC IN THE CENTER OF THE STRUCTURE * /
COMMENT * BENEATH THE SLOT * /
DIELECTRIC NO NULL 5.5 0.0 0.0 17 22 6 10 1 3 /
DIELECTRIC NO NULL 5.5 0.0 0.0 17 22 31 35 1 3  /
DIELECTRIC NO NULL 5.5 0.0 0.0 17 22 6 10 7 11 /
DIELECTRIC NO NULL 5.5 0.0 0.0 17 22 31 35 7 11/
```

```
DIELECTRIC NO NULL 5.5 0.0 0.0 17 22 6 10 15 17 /
DIELECTRIC NO NULL 5.5 0.0 0.0 17 22 31 35 15 17 /


COMMENT *FORM THE BEAMHOLE * /
STRUCTURE ELLIPTICAL BEAMFILL +1 CARTESIAN .0018453 .0016383 0.0
                                .0018453 .0016383 .000635
                                 1 0 0 .00046175 .00033655
                                 1 0 0 .00046175 .00033655
                                 0 360 0 360 /


STRUCTURE ELLIPTICAL BEAMHOLE -1 CARTESIAN .0018453 .0016383 0.0
                                .0018453 .0016383 .000635
                                 1 0 0 .00043 .0003048
                                 1 0 0 .00043 .0003048
                                 0 360 0 360/

STRUCTURE ELLIPTICAL SLOT1 -1 CARTESIAN .0018453 .0016383 .0000762
                                .0018453 .0016383 .0002413
                                 1 0 0 .00046175 .00033655
                                 1 0 0 .00046175 .00033655
                                 0 360 0 360 /

STRUCTURE ELLIPTICAL SLOT2 -1 CARTESIAN .0018453 .0016383 .0003937
                                .0018453 .0016383  .0005588
                                 1 0 0 .00046175 .00033655
                                 1 0 0 .00046175 .00033655
                                 0 360 0 360 /

COMMENT * FORM THE LADDER * /
STRUCTURE CONFORMAL LADDERLEFT +1 0 10 19 22 1 17 /
STRUCTURE CONFORMAL LADDERRIGHT +1 29 39 19 22 1 17 /
STRUCTURE CONFORMAL SLOT3 -1 1 10 19 22 2 8 /
STRUCTURE CONFORMAL SLOT5 -1 29 38 19 22 2 8 /
STRUCTURE CONFORMAL SLOT7 -1 1 10 19 22 10 16 /
STRUCTURE CONFORMAL SLOT9 -1 29 38 19 22 10 16 /


SYMMETRY MIRROR          +1 1 38 1 40 1 1 /


FREQUENCY 2 35E+9 .005 50000 /

BALANCE 1 1 38 1 40 1 17 /
OBSERVE 1 YES ENERGY 1 0.0 0.0 0.0 0.0 TOTAL 0 1 /

LINPRINT 1 3 2 1 19 19 20 20 1 17 0 0 1 0 0 0 0 0 0 /
RANGE    1 1 0 0 3 19 19 20 20 1 17 /

START /
STOP /
```

REPORT DOCUMENTATION PAGE

Form Approved
OMB No. 0704-0188

1. AGENCY USE ONLY *(Leave blank)*

2. REPORT DATE
March 1993

3. REPORT TYPE AND DATES COVERED
Technical Paper

4. TITLE AND SUBTITLE
Simulation of TunneLadder Traveling-Wave Tube Cold-Test Characteristics: Implementation of the Three-Dimensional, Electromagnetic Circuit Analysis Code Micro-SOS

5. FUNDING NUMBERS
WU 506-44-2B

6. AUTHOR(S)
Carol L. Kory and Jeffrey D. Wilson

7. PERFORMING ORGANIZATION NAME(S) AND ADDRESS(ES)
National Aeronautics and Space Administration
Lewis Research Center
Cleveland, Ohio 44135-3191

8. PERFORMING ORGANIZATION REPORT NUMBER
E-7008

9. SPONSORING/MONITORING AGENCY NAMES(S) AND ADDRESS(ES)
National Aeronautics and Space Administration
Washington, D.C. 20546-0001

10. SPONSORING/MONITORING AGENCY REPORT NUMBER
NASA TP-3294

11. SUPPLEMENTARY NOTES
Carol L. Kory, Ohio Aerospace Institute, 2001 Aerospace Parkway, Brook Park, Ohio 44142; Jeffrey D. Wilson, NASA Lewis Research Center. Responsible person, Jeffrey D. Wilson, (216) 433-3513.

12a. DISTRIBUTION/AVAILABILITY STATEMENT
Unclassified - Unlimited
Subject Category 33

12b. DISTRIBUTION CODE

13. ABSTRACT ***(Maximum 200 words)***

The three-dimensional, electromagnetic circuit analysis code, Micro-SOS, can be used to reduce expensive and time-consuming experimental "cold-testing" of traveling-wave tube (TWT) circuits. The frequency-phase dispersion characteristics and beam interaction impedance of a TunneLadder traveling-wave tube slow-wave structure were simulated using the code. When reasonable dimensional adjustments are made, computer results agree closely with experimental data. Modifications to the circuit geometry that would make the TunneLadder TWT easier to fabricate for higher frequency operation are explored.

14. SUBJECT TERMS
TunneLadder; Traveling-wave tube

15. NUMBER OF PAGES
16

16. PRICE CODE
A03

17. SECURITY CLASSIFICATION OF REPORT	18. SECURITY CLASSIFICATION OF THIS PAGE	19. SECURITY CLASSIFICATION OF ABSTRACT	20. LIMITATION OF ABSTRACT
Unclassified	Unclassified	Unclassified	